

Fullerene-Mediated Aggregation of $M_{25}(SR)_{18}^-$ ($M = Ag, Au$) Nanoclusters

Papri Chakraborty, Abhijit Nag, Biswajit Mondal, Esmā Khatun, Ganesan Paramasivam, and Thalappil Pradeep*

Cite This: *J. Phys. Chem. C* 2020, 124, 14891–14900

Read Online

ACCESS |

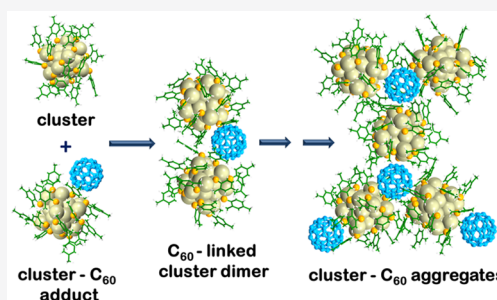
Metrics & More

Article Recommendations

Supporting Information

ABSTRACT: We report fullerene (C_{60} and C_{70})-induced aggregation of atomically precise clusters, taking $M_{25}(SR)_{18}^-$ ($M = Ag, Au$ and $-SR$ is a thiolate ligand) clusters as an example. We show that dimers, trimers, tetramers, and even higher aggregates of the clusters can be created by supramolecular interaction with fullerenes. Adducts such as $[\{M_{25}(SR)_{18}\}_n(C_{60})]^{n-}$ ($n = 1-5$), $[\{M_{25}(SR)_{18}\}_n(C_{60})_{n-1}]^{n-}$ ($n = 2-5$), and $[\{M_{25}(SR)_{18}\}_n(C_{60})_n]^{n-}$ ($n = 1, 2, 3, \dots$, etc.) were formed, which were studied by electrospray ionization mass spectrometry. Similar adducts with C_{70} were also observed. Structural insights were obtained from molecular docking and density functional theory calculations. Computational studies predicted the possibility of isomerism in some of these adducts. Fullerenes linked multiple clusters, causing aggregation.

Fullerenes and clusters formed host–guest complexes in such assemblies. The possibilities of coassembly between the clusters and the fullerenes were also studied in the solid state. The nature of adducts observed in the case of $M_{25}(SR)_{18}^-$ was completely different compared to the previously reported fullerene adducts of $[Ag_{29}(BDT)_{12}]^{3-}$ (where BDT is 1,3-benzene dithiol), in which multiple fullerenes were attached on the surface of a single cluster. Supramolecular aggregates formed in the case of $M_{25}(SR)_{18}^-$ were independent of the nature of the metal atoms (Ag or Au). This implied that for an appropriate geometry of the cluster weak interactions with the ligands and ion-induced dipole interactions were more important in controlling the complexation compared to the metallophilic interactions. Exploring the interaction of atomically precise clusters with fullerenes is important, as the resulting adducts can show new properties such as isomerism, chirality, charge transfer, or enhanced optical properties.



INTRODUCTION

Monolayer protected atomically precise nanoclusters show unique properties and find applications in numerous fields including catalysis, sensing, energy, etc.^{1–9} These clusters show molecular behavior which is reflected in their optical absorption features. X-ray crystallography is widely used to determine their structures.^{1,10–12} Such clusters are also characterized by using mass spectrometry (MS).^{13,14} Monolayers of ligands, capping the metal core of the cluster, can interact with other molecules. This has enabled the possibilities of exploring supramolecular chemistry of such clusters.^{15–20} There can be intracuster and intercluster interactions that can form different types of self-assembled structures. These interactions play an active role in their packing in crystals.^{16,17,21,22} Nag et al. reported that intercluster interactions were responsible for polymorphism in the crystal packing of $[Ag_{29}(BDT)_{12}(PPh_3)_4]^{3-}$ (BDT is 1,3-benzene dithiol and PPh_3 is triphenyl phosphine) clusters.²³ Zheng et al. showed how the protecting ligands of $Au_{246}(p-MBT)_{80}$ ($p-MBT$ is a *para*-mercapto benzene thiol) formed different patterns on the cluster surface.²¹ Intercluster interactions can also result in aggregation of clusters. Dimers and trimers of $[Au_{25}(SR)_{18}]^-$ ($-SR$ is a thiolate ligand) were observed in the

gas phase, which were favored due to the aurophilic interactions between the clusters.²⁴ $Au_{25}(SBU)_{18}$ (SBU is *n*-butanethiolate) clusters were also found to be connected by Au–Au bonds and exist as linear polymers in their crystal structure.²⁵ Recently, Hossain et al. reported one-dimensional structures of $Au_4Pt_2(SR)_8$ clusters which were also connected via Au–Au bonds.²⁶ Wen et al. reported one-dimensional polymers of $[Au_7Ag_9(dppf)_3(CF_3CO_2)_7BF_4]_n$ (dppf is 1,10-bis(diphenylphosphino)ferrocene), which were connected linearly via Ag–O bonds.²⁷ Chakraborty et al. reported that dimerization of clusters can also be induced by alkali metal ions, as observed in $[Ag_{29}(BDT)_{12}(PPh_3)_4]^{3-}$.²⁸ Wei et al. further demonstrated that interaction of Cs^+ with $[Ag_{29}(BDT)_{12}(PPh_3)_4]^{3-}$ modified its geometric structure by stripping off the PPh_3 ligands and induced the formation of intercluster assemblies by arranging the clusters into one-

Received: April 16, 2020

Revised: June 9, 2020

Published: June 10, 2020



dimensional arrays in their crystal lattice.²⁹ Chandra et al. reported self-assembly of water-soluble Au clusters into spherical colloidal superstructures with high photocatalytic activity and applications in bioimaging by utilizing the interaction of the clusters with Sn²⁺ ions.³⁰ Other cations like Zn²⁺ were also used to study phenomena such as aggregation-induced emission in Au clusters.^{31,32} Anionic templates like CO₃²⁻ were used to link Ag₁₇S₈ clusters into a two-dimensional (2D) honeycomb-like structure.³³ Nonappa et al. reported the formation of spherical capsids and 2D monolayer thick sheets of clusters which were formed due to weak hydrogen bonding interactions.³⁴ Apart from these, aggregates of clusters were also created by covalent linkages.^{35–38} Such covalent bonding between clusters was extended to create cluster-based metal–organic frameworks (MOFs).^{39–41} Moreover, encapsulation of clusters into common MOFs like ZIF-8 and ZIF-67 occurred due to electrostatic interactions, and such hybrid materials found application in CO₂ conversion.⁴²

Recent studies are also focusing on the interaction of clusters with other molecules like cyclodextrins (CD),^{43–46} fullerenes,⁴⁷ and crown ethers.⁴⁸ Mathew et al. reported host–guest complexes of Au₂₅(SBB)₁₈[−] (SBB is 4-(*t*-butyl)benzyl thiolate) clusters with CDs,⁴³ and Nag et al. reported supramolecular complexes of [Ag₂₉(BDT)₁₂]₃[−] clusters with CDs.⁴⁴ Chakraborty et al. studied the interaction between [Ag₂₉(BDT)₁₂]₃[−] and fullerenes.⁴⁷ In all these cases, the complexes were primarily stabilized by weak supramolecular forces.¹⁵ Co-crystallization of [Ag₂₉(BDT)₁₂(PPh₃)₄]₃[−] clusters and crown ethers was also achieved.⁴⁸ Such supramolecular complexes are particularly interesting due to the additional properties that can be incorporated into the cluster system due to the complexation with the heteromolecules.^{15,16} In most cases, such complexation enhanced the stability of the clusters. Isomerism was observed in the host–guest complexes, [Ag₂₉(BDT)₁₂(CD)_{*n*}]₃[−] (*n* = 1–6).⁴⁴ Recently, Muhammad et al. reported pilla[5]arene-capped silver clusters.⁴⁹ The pilla[5]arene macrocycles on the surface of the cluster were available for taking part in further host–guest complexation which modified the optical properties of the nanoclusters.⁴⁹ Self-assembly of clusters has thus emerged as an effective way to vary their optical and luminescence properties.⁵⁰ Due to such possibilities, studies on supramolecular chemistry of atomically precise clusters have attracted researchers in recent times.

Fullerenes are known to form numerous host–guest complexes and can also bring in properties like superconductivity, metallicity, charge transfer, etc., in their hybrid composites.^{51–53} Superatomic crystals containing inorganic clusters and fullerenes are particularly important for studying electron transport properties.⁵⁴ Several such fullerene-containing superatomic crystals, e.g., [Co₆Se₈(PET₃)₆][C₆₀]₂, [Ni₉Te₆(PET₃)₈][C₆₀], [Cr₆Te₈(PET₃)₆][C₆₀]₂, etc., have been reported in the literature.⁵⁵ However, studies of interaction between ligand-protected noble metal clusters and fullerenes are still limited. One of the reports showed that intercluster compounds, [Au₇(PPh₃)₇]₂C₆₀·THF and [Au₈(PPh₃)₈](C₆₀)₂, were stabilized primarily by π – π , C–H \cdots π , and Coulomb interactions between the Au clusters and the fullerenes.⁵⁶ Earlier, we had reported supramolecular complexes of [Ag₂₉(BDT)₁₂]₃[−] with fullerenes.⁴⁷ The adducts, [Ag₂₉(BDT)₁₂(C₆₀)_{*n*}]₃[−] (*n* = 1–9), were formed due to weak supramolecular interactions. C₆₀ molecules were captured

into appropriate cavities on the surface of the cluster. Thus, the structure of the cluster played a significant role in controlling host–guest complexation. These unfolded the possibilities of studying the interaction of fullerenes with a variety of clusters. Depending on the inherent geometry of the nanocluster, the nature of the metal atoms, and the monolayer of the ligands, the nature of complexation is expected to vary which can produce a wide range of such cluster–fullerene complexes.

In this work, we investigated the interaction of C₆₀ and C₇₀ with two archetypical atomically precise clusters, [Ag₂₅(DMBT)₁₈]_− (DMBT is 2,4-dimethylbenzene thiol)⁵⁷ and [Au₂₅(PET)₁₈]_− (PET is 2-phenyl ethanethiol),^{10,58} which have the same core structure but protected by different ligands. Fullerene-induced aggregation of the clusters was observed in both cases, and the nature of the complexation was independent of the nature of the metal atoms. Fullerene-mediated dimers, trimers, tetramers, and even higher aggregates of the clusters were formed due to supramolecular interactions between the cluster and the fullerenes. The complexation was studied using electrospray ionization mass spectrometry (ESI MS), and greater insights into the nature of binding were obtained from collision-induced dissociation (CID). We used molecular docking and density functional theory (DFT) to predict the structure of the adducts. The nature of adducts observed in the case of [Ag₂₅(DMBT)₁₈]_− and [Au₂₅(PET)₁₈]_− was distinct, compared to that of the fullerene adducts of [Ag₂₉(BDT)₁₂]₃[−], reported earlier.⁴⁷ In the case of [Ag₂₉(BDT)₁₂]₃[−], the surface of an isolated cluster was functionalized by numerous fullerenes.⁴⁷ In contrast, in the case of [M₂₅(SR)₁₈]_− (M = Ag, Au), multiple clusters self-assembled to form larger aggregates by interaction with fullerene molecules. This study clearly reveals how a variety of cluster–fullerene adducts can be created by choosing the appropriate system of clusters and also how cluster aggregates can be created by supramolecular interaction with heteromolecules.

■ EXPERIMENTAL SECTION

Materials and Methods. All the reagents used for the synthesis of the clusters were commercially available. Silver nitrate (AgNO₃) was procured from Rankem, India. The thiols 2,4 -DMBT and PET were purchased from Sigma-Aldrich. Sodium borohydride (NaBH₄), tetraphenyl phosphonium bromide (PPh₄Br), tetrabutyl ammonium bromide (TOABr), PPh₃, and fullerenes (C₆₀ and C₇₀) were obtained from Sigma-Aldrich. Chloroauric acid (HAuCl₄·3H₂O) was synthesized in the laboratory starting from pure metallic gold (24 carat). The solvents used, namely, methanol (MeOH), dichloromethane (DCM), toluene, and acetone, were of HPLC grade.

Instrumentation. A PerkinElmer Lambda 25 UV–vis spectrophotometer was used to measure the optical absorption spectra. The ESI MS measurements were done using a Waters Synapt G2 Si mass spectrometer. All the spectra were collected in the negative ion mode. ESI MS measurements were done using the following instrumental parameters: capillary voltage, 3 kV; cone voltage, 0; source offset, 0; trap gas, 8 mL/min; source and desolvation temperature, 150 °C. A JEOL 3010 instrument was used for performing the transmission electron microscopy (TEM) studies.

Synthetic Protocol of [Ag₂₅(DMBT)₁₈]_− Clusters. [Ag₂₅(DMBT)₁₈]_− clusters were synthesized according to the method reported by Joshi et al.⁵⁷ About 38 mg of AgNO₃ and 90 μ L of the thiol, 2,4-DMBT, were dissolved in about 18 mL

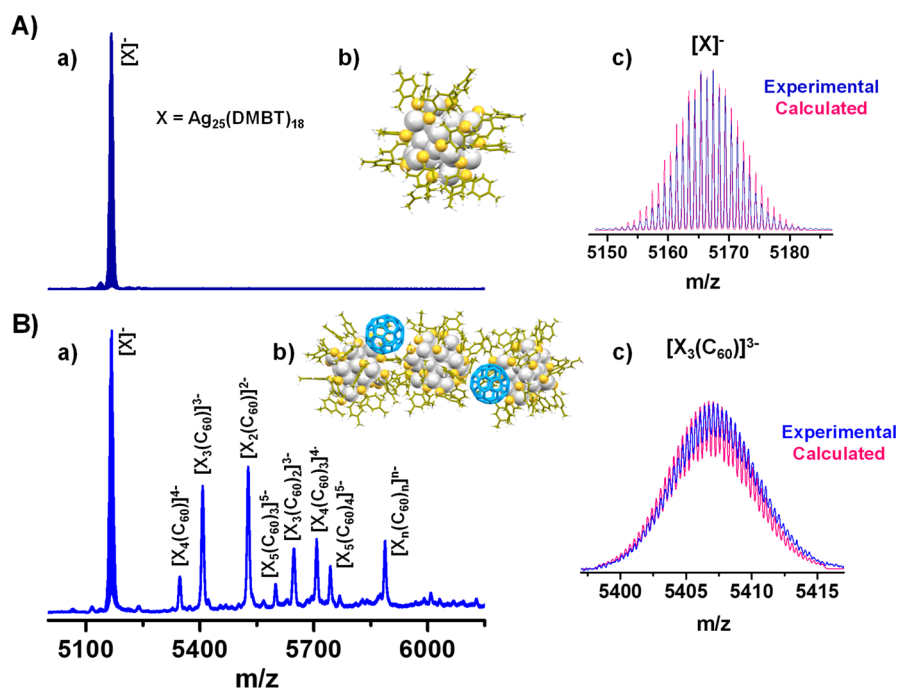


Figure 1. (A) (a) ESI MS of X^- , (b) structure of X^- (computed using coordinates from the crystal structure), and (c) experimental and theoretical isotopic patterns of X^- . (B) (a) ESI MS showing the adducts of X^- and C_{60} , (b) schematic showing an aggregate of X^- with C_{60} , and (c) experimental and theoretical isotopic patterns of one of the adducts, $[X_3(C_{60})]^{3-}$ [$X = Ag_{25}(DMBT)_{18}$]. Color codes: gray, Ag; yellowish-green, C; yellow, S; white, H; blue, fullerenes.

of a solvent mixture of MeOH and DCM (MeOH:DCM = 1:8) to allow the formation of yellow-colored Ag thiolates. The reaction was maintained at 0 °C and was stirred at 900 rpm. About 15 min later, ~6 mg of PPh_4Br , dissolved in ~0.5–1 mL of MeOH, was added to the reaction mixture. Next, about 2–3 min later, 15 mg $NaBH_4$, dissolved in ~0.5 mL of ice-cold water, was added dropwise. Upon addition of $NaBH_4$, the color of the solution changed to brown. The reaction mixture was stirred at 0 °C for about 8 h and then was kept in the freezer at 4 °C for about 2 days. Then, the crude mixture containing the clusters was purified. First, the mixture was centrifuged, and the precipitate was separated. Next, DCM was evaporated from the supernatant, and the resulting solid was cleaned by washing with MeOH. The solid cluster was then dissolved in DCM and centrifuged. The purified clusters were then obtained in powder form by removing DCM by rotary evaporation.

Synthetic Protocol of $[Au_{25}(PET)_{18}]^-$ Clusters. $[Au_{25}(PET)_{18}]^-$ clusters were made by slightly altering an already reported protocol.^{59,60} About 40 mg of the Au precursor, $HAuCl_4 \cdot 3H_2O$, was dissolved in ~8 mL of THF and mixed with 65 mg of TOABr. The solution was then stirred for 15–20 min. After about 1 h, ~68 μL of PET was introduced into the reaction mixture under stirring conditions, which caused the formation of Au thiolates. Next, about 40 mg of $NaBH_4$ (in ice-cold water) was added. Then the reaction was kept under stirring for another 5–6 h to allow size-focusing of the clusters. The clusters were then dried by rotary evaporation followed by washing the dried cluster with MeOH. Then, the pure clusters were extracted using acetone and centrifuged, and the precipitate was discarded. The supernatant containing the pure clusters was then vacuum-dried and stored for further use.

Computational Details. Molecular docking was done to determine the structure of the cluster–fullerene adducts. The

Lamarckian genetic algorithm in the Autodock 4.2 program⁶¹ was used for this purpose. The lowest energy structures obtained from docking were further optimized using DFT. DFT calculations were done using the grid-based projector-augmented wave (GPAW) method.^{62,63} The Perdew–Burke–Ernzerhof (PBE) functional⁶⁴ was used in our calculations. Double zeta plus polarization (DZP) was used as the basis set in the linear combination of atomic orbitals (LCAO) method. The crystal structure of $Ag_{25}(DMBT)_{18}^-$ was used as the initial structure⁵⁷ for carrying out the computational work. The binding energies (B.E.s) of the adducts were calculated by deducting the free energies of the isolated clusters and fullerenes from the total energies of the adducts by using the following formula: $B.E._{adduct} = E_{adduct} - (xE_{cluster} + yE_{fullerene})$, where x and y are the number of clusters and fullerenes in the adduct, respectively. E_{adduct} , $E_{cluster}$, and $E_{fullerene}$ are the lowest energies of the DFT-optimized structures of the adduct, isolated clusters, and isolated fullerenes (C_{60}/C_{70}), respectively.

RESULTS AND DISCUSSION

Supramolecular Interaction of $Ag_{25}(DMBT)_{18}^-$ with C_{60} . $[Ag_{25}(DMBT)_{18}]^-$ was synthesized according to the method discussed above in the experimental part and further characterized using UV–vis (Figure S1) and ESI MS (Figure 1Aa).⁵⁷ As such data have been published before,⁵⁷ we are presenting only essential data in the main text. $Ag_{25}(DMBT)_{18}$ is referred to as X in the subsequent discussion. Fullerene adducts of the cluster were prepared by mixing solutions of C_{60} (in toluene) and X^- (in DCM). The parent cluster ion, X^- , appeared as a peak at m/z 5167 (Figure 1Aa), and its theoretical and experimental isotopic distributions are presented in the inset (c) of Figure 1A. The structure of the cluster is shown in inset (b) of Figure 1A. The structure was

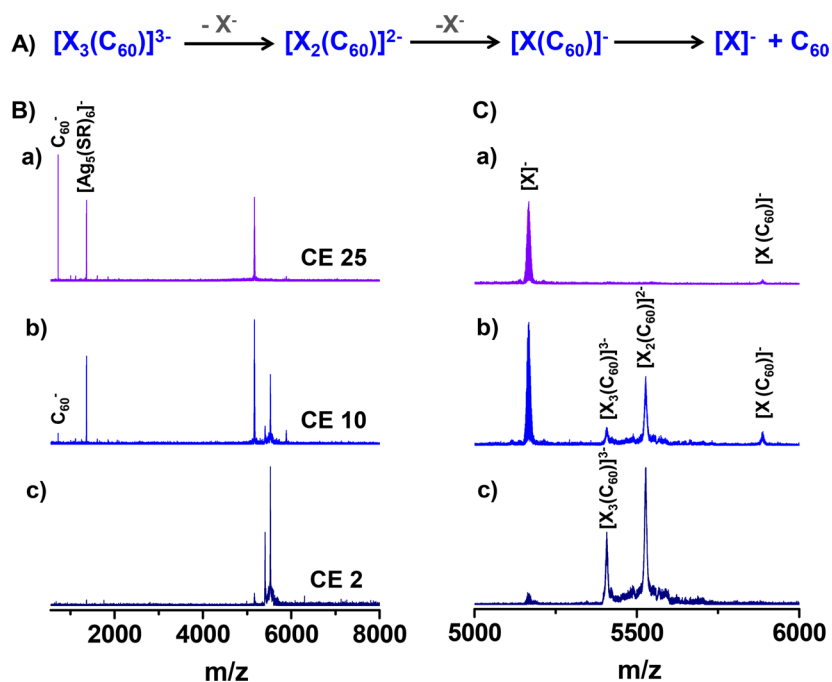


Figure 2. (A) Fragmentation pathway of the adduct, $[X_3(C_{60})]^{3-}$ [$X = Ag_{25}(DMBT)_{18}$]. (B) CID mass spectra of $[X_3(C_{60})]^{3-}$ and (C) expanded views showing the products of CID in the m/z range of 5000–6000 at varying C.E.s of 2 (c), 10 (b), and 25 (a). C.E. is in instrumental unit.

optimized using DFT, with initial inputs from the crystal structure.⁵⁷ Upon addition of C_{60} , several new peaks were observed in ESI MS in the m/z range of 5250–6000 (see Figure 1Ba), which corresponded to the cluster–fullerene complexes. Detailed analysis of the peaks revealed the composition of the adducts as $[X_4(C_{60})]^{4-}$ (m/z 5347), $[X_3(C_{60})]^{3-}$ (m/z 5407), $[X_2(C_{60})]^{2-}$ (m/z 5527), $[X_5(C_{60})_3]^{5-}$ (m/z 5599), $[X_3(C_{60})_2]^{3-}$ (m/z 5647), $[X_4(C_{60})_3]^{4-}$ (m/z 5707), and $[X_5(C_{60})_4]^{5-}$ (m/z 5743). The composition of some of these adducts may be generalized, such as $[X_n(C_{60})]^{n-}$ ($n = 1–4$) and $[X_n(C_{60})_{n-1}]^{n-}$ ($n = 2–5$). Adducts with further higher values of n were not observed in this case. Probably, such higher adducts were not stable due to Coulombic repulsions between the clusters. The compositions were determined by analyzing the m/z values, charge states, and isotopic patterns of the peaks. The isotopic distribution of the peak for one of these adducts, $[X_3(C_{60})]^{3-}$, is presented in the inset (c) of Figure 1B. The difference between the peaks in the isotopic distribution is m/z 0.33, which confirmed a charge state of 3 $-$. The experimental isotopic distribution was comparable to the calculated isotopic distribution of $[X_3(C_{60})]^{3-}$, which further confirmed its composition. However, an important aspect to note is the drastic loss of resolution of the adducts, in comparison to the parent cluster, which is partly attributed to the higher charge state of the adducts. ESI MS suggested the attachment of neutral fullerenes to the cluster, but the nature of these adducts was completely different compared to the fullerene adducts of $[Ag_{29}(BDT)_{12}]^{3-}$, reported earlier.⁴⁷ In the case of $[Ag_{29}(BDT)_{12}(C_{60})_n]^{3-}$ ($n = 1–9$), the fullerenes covered the surface of a single cluster. For X^- , in contrast, fullerene-induced aggregation of the clusters occurred. Multiple fullerene attachment to a single cluster was not observed in the case of X^- . The adduct $[X_2(C_{60})]^{2-}$ was a fullerene-mediated dimer of the cluster. Similarly, the adducts, $[X_3(C_{60})]^{3-}$ and $[X_3(C_{60})_2]^{3-}$, were trimers, and $[X_4(C_{60})]^{4-}$ and

$[X_4(C_{60})_3]^{4-}$ were tetramers of the cluster. The peak at m/z 5887 was assigned as $[X_n(C_{60})_n]^{n-}$ ($n = 1, 2, 3, \dots$, etc.). However, due to the poor isotopic resolution of the peak, the limiting value of n could not be determined accurately. A schematic of aggregate formation between the cluster and C_{60} is presented in the inset (b) of Figure 1B. Optical absorption showed a slight increase in the absorbance of the cluster upon addition of C_{60} (Figure S2A), reflecting the effect of such supramolecular complexation in solution. Additional scattering of light by the particulates in the solution may have also resulted in such a phenomenon. However, addition of C_{60} did not show any significant effect on the emission properties of the cluster (Figure S2B). The cluster–fullerene aggregates were stable when stored under cold conditions at 4 °C, as observed from their optical absorption spectrum, which was almost unaltered even after 7 days (Figure S3).

CID Studies of the Fullerene Adducts of X^- . We performed CID to get further insights into the structure of these adducts. The peak of the adduct, $[X_3(C_{60})]^{3-}$, was mass-selected and subjected to collision with Ar gas, confined in the trap chamber of the mass spectrometer. Upon increasing the collision energy (C.E.), stepwise loss of the cluster, X^- , from the adduct $[X_3(C_{60})]^{3-}$ (see Figure 2) was observed. The fragmentation pathway is presented in Figure 2A. In the first step, loss of X^- from $[X_3(C_{60})]^{3-}$ resulted in the formation of $[X_2(C_{60})]^{2-}$. Upon increasing the C.E., further loss of X^- resulted in the formation of $[X(C_{60})]^-$. Finally, at higher C.E.s, X^- and C_{60}^- were formed. C_{60}^- was probably formed by charge transfer from X^- to C_{60} .⁴⁷ Along with C_{60}^- , X was also formed in this charge transfer process, which being a neutral species was not detected in ESI MS. The CID mass spectra with increasing C.E.s are presented in Figure 2B, and expanded views of the fragment peaks in the m/z range of 5000–6000 of the corresponding spectra are presented in Figure 2C. At C.E. of 2 also, some extent of fragmentation of $[X_3(C_{60})]^{3-}$ to $[X_2(C_{60})]^{2-}$ was observed, as supramolecular adducts are weak

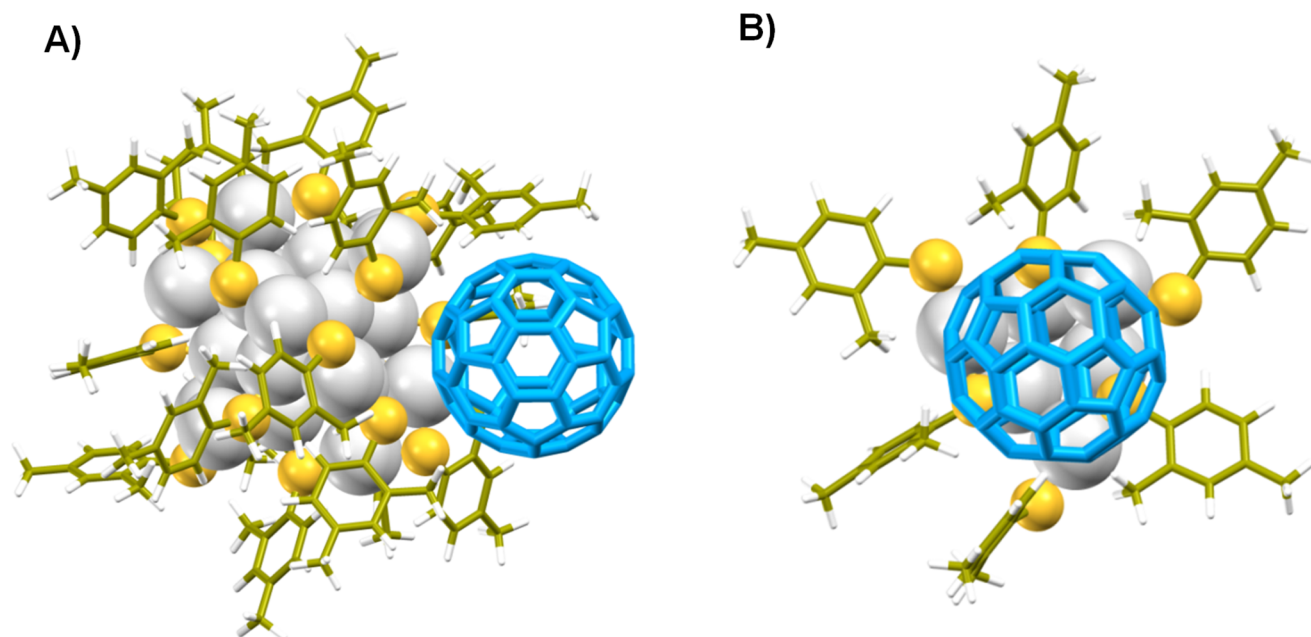


Figure 3. (A) Lowest energy structure of the adduct, $[X(C_{60})]^-$ [$X = Ag_{25}(DMBT)_{18}$], obtained from DFT. (B) Enlarged view of the interaction between C_{60} attached on the cluster surface and the neighboring DMBT ligands.

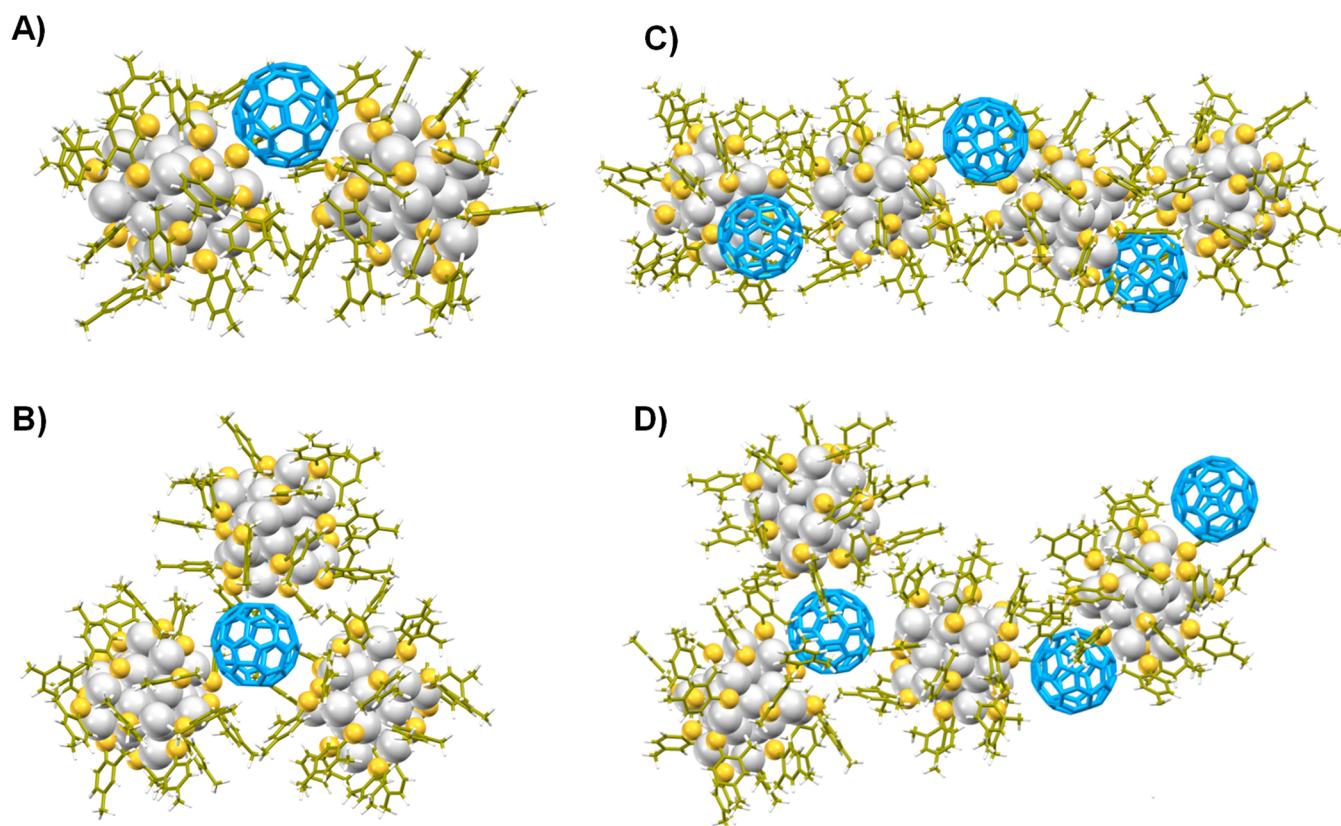


Figure 4. Lowest energy structures of (A) $[X_2(C_{60})]^{2-}$ and (B) $[X_3(C_{60})]^{3-}$. Two isomeric structures of $[X_4(C_{60})_3]^{4-}$ are in (C) and (D) [$X = Ag_{25}(DMBT)_{18}$].

and fragmentation occurs even without any applied C.E. The peak observed for $Ag_5(SR)_6^-$ was due to the usual fragmentation of the parent cluster.⁶⁵ CID studies also revealed the distinct binding modes of complexation of C_{60} and X^- , compared to that of the previously reported C_{60} adducts of $[Ag_{29}(BDT)_{12}]^{3-}$.⁴⁷ In the case of $[Ag_{29}(BDT)_{12}(C_{60})_n]^{3-}$ ($n =$

1–4), where the nanocluster surface was covered by fullerenes, sequential loss of C_{60} was observed.⁴⁷ In contrast, in the case of the adduct $[X_3(C_{60})]^{3-}$, sequential loss of the clusters, X^- , was observed, and C_{60} was lost only in the final stages. This implied that in the structure of $[X_3(C_{60})]^{3-}$, C_{60} was probably encapsulated by three clusters. CID of the other adducts like

$[X_4(C_{60})]^{4-}$, presented in Figure S4, also showed similar fragmentation sequence. Also, at low C.E., $[X_4(C_{60})]^{4-}$ showed extensive fragmentation to $[X_3(C_{60})]^{3-}$, $[X_2(C_{60})]^{2-}$, and $[X]^-$ indicating that the smaller adducts like $[X_3(C_{60})]^{3-}$ and $[X_2(C_{60})]^{2-}$ were probably fragments of the larger adducts.

Computational Studies to Determine the Structure of Adducts of X^- with C_{60} . We carried out molecular docking followed by DFT calculations to investigate the structure of the adducts of C_{60} and X^- . To determine the lowest energy geometry of the adduct $[X(C_{60})]^-$, X^- was used as the receptor, and C_{60} was used as the free ligand in docking. As molecular docking primarily considers the supramolecular interactions, the lowest energy geometry of $[X(C_{60})]^-$, obtained from molecular docking, was further optimized using DFT to consider the electronic factors too. The lowest energy structure of $[X(C_{60})]^-$ (Figure 3A) showed that C_{60} was captured in a cavity on the cluster surface which was enclosed by six 2,4-DMBT ligands. An expanded view of the interactions between the six DMBT ligands and C_{60} , attached on the cluster surface, is presented in Figure 3B. DFT calculations revealed a binding energy (B.E.) of -10.25 kcal/mol for this adduct. Here, the major forces stabilizing the complex were vdW interactions and $C-H\cdots\pi$ contacts between the $-H$ of $-CH_3$ groups of the ligands and the π -system of C_{60} . Moreover, it is well-known that metal clusters can also bind to fullerene surfaces.⁶⁶ From Figure 3, it is clear that there were strong contacts between the Ag atoms of the cluster and C_{60} , which contributed ion-induced dipole interactions to the overall stabilization of the complex. Similarly, the structures of the larger adducts were also determined. To determine the structure of $[X_2(C_{60})]^{2-}$, the lowest energy structure of $[X(C_{60})]^-$ was chosen as the receptor, and another X^- was chosen as the free ligand in docking. The lowest energy geometry of $[X_2(C_{60})]^{2-}$ (Figure 4A) showed that C_{60} interacted with DMBT ligands of two clusters. Similarly, the structure of $[X_3(C_{60})]^{3-}$ was obtained by docking $[X_2(C_{60})]^{2-}$ with X^- . The lowest energy structure of $[X_3(C_{60})]^{3-}$ (Figure 4B) revealed that C_{60} was indeed encapsulated by three X^- clusters. The surface of C_{60} was covered by the clusters, and as the clusters remained exposed, they were the first ones to be lost upon increasing C.E. during the CID experiments. The B.E.s for the adducts $[X_2(C_{60})]^{2-}$ and $[X_3(C_{60})]^{3-}$ were -9.80 kcal/mol and -3.86 kcal/mol, respectively. The lower B.E. in the case of $[X_3(C_{60})]^{3-}$ may be attributed to steric factors and an increase in repulsion between the negatively charged clusters, which may reduce the favorable $C-H\cdots\pi$ interactions.

The structures of the heavier adducts, $[X_n(C_{60})_{n-1}]^{n-}$ ($n = 3-4$), were obtained only from molecular docking, due to the computational cost involved in DFT. These structures showed two isomeric possibilities in each case. The two isomeric forms of the adduct, $[X_4(C_{60})_3]^{4-}$, are presented in Figure 4C and 4D, respectively, where the structure shown in Figure 4D exhibited a greater extent of branching. Similar possibilities of isomerism in the structures of the other adducts like $[X_3(C_{60})_2]^{3-}$ are presented in Figure S5. In the structures of $[X_n(C_{60})]^{n-}$ ($n = 1-3$) and $[X_n(C_{60})_{n-1}]^{n-}$ ($n = 2-4$), some C_{60} 's were enclosed by the clusters. However, equivalent sites on the cluster surface were free and accessible for the capture of more fullerenes which could further bind more clusters. Thus, these assemblies could extend further, leading to the formation of larger aggregates of such cluster–fullerene complexes.

We further examined the possibilities of such aggregation in the solid state by using TEM. Solutions of cluster–fullerene complexes were drop-casted on TEM grids and examined. TEM studies revealed that the cluster–fullerene adducts were assembled into wire-like structures in the solid state (Figure S6A,B), which was in accordance with the nature of the complexation observed in ESI MS and the structures predicted from theoretical studies. Self-assembly of individual nanoclusters into such a dendritic network of micrometer dimension was recently observed by Musnier et al. by incorporating anisotropic surface charges on atomically precise gold clusters.⁶⁷ Here, fullerenes might also act as anisotropic targets, leading to similar assemblies. However, under identical conditions, the parent clusters also assembled into a mixture of wire-like and sheet-like structures (Figure S6C,D). This implied that probably fullerenes enhanced the formation of the linear assemblies of the clusters, resulting in the formation of uniform wire-like structures in the solid state. Specifically, the ion-induced dipole interactions between the Ag atoms of the cluster and C_{60} might have enhanced the nanowire formation. However, the positions of C_{60} and the clusters in the assemblies were not resolved from TEM. So, this aspect of assembly formation in the solid state was not probed in further detail in the current study.

Supramolecular Interaction of X^- with C_{70} . We further investigated the interaction of X^- with ellipsoidal-shaped C_{70} . The similar nature of adducts of C_{70} with X^- was observed in ESI MS. The adducts, $[X_4(C_{70})]^{4-}$ (m/z 5376), $[X_3(C_{70})]^{3-}$ (m/z 5446), $[X_2(C_{70})]^{2-}$ (m/z 5586), $[X_5(C_{70})_3]^{5-}$ (m/z 5670), $[X_3(C_{70})_2]^{3-}$ (m/z 5726), $[X_4(C_{70})_3]^{4-}$ (m/z 5796), $[X_5(C_{70})_4]^{5-}$ (m/z 5838), and $[X_n(C_{70})_n]^{n-}$ (m/z 6006), were formed, as presented in Figure 5(a). Comparison of the

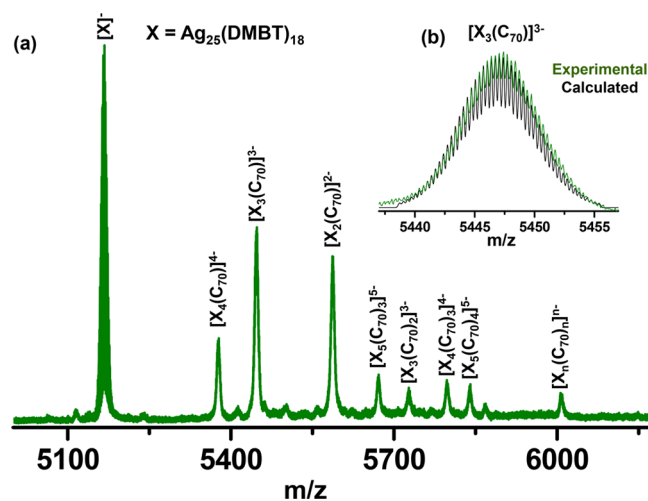


Figure 5. ESI MS showing the adducts of X^- and C_{70} is shown in (a). Inset (b) shows the experimental and theoretical isotopic patterns of one of the adducts, $[X_3(C_{70})]^{3-}$ [$X = Ag_{25}(DMBT)_{18}$].

experimental and calculated isotopic distributions of one of these adducts, $[X_3(C_{70})]^{3-}$, is presented in the inset (b) of Figure 5. We also performed molecular docking followed by DFT calculations to determine the structure of $[X(C_{70})]^-$. The lowest energy structure, obtained from molecular docking, showed that C_{70} interacted at a similar site on the cluster surface with its major axis oriented toward the cluster (Figure S7A). The complexation was also stabilized by vdW, $C-H\cdots\pi$, and ion-induced dipole interactions. DFT revealed a B.E. value

of -7.29 kcal/mol for the adduct, $[X(C_{70})]^-$. However, we also constructed another isomeric structure of $[X(C_{70})]^-$ with the minor axis of C_{70} projected toward the cluster and optimized it in DFT (Figure S7B). The B.E. in the case of this isomer was -6.15 kcal/mol, which was slightly lower compared to the B.E. obtained for the lowest energy isomer. The lower B.E.s in the case of C_{70} compared to that of C_{60} revealed that larger-sized fullerenes allowed lesser interaction in the case of X^- . C_{70} also induced the formation of dendritic assemblies of the cluster in the solid state (Figure S8), but these assemblies were less uniform in their wire-like morphology compared to that of the assemblies of C_{60} .

Supramolecular Interaction of $Au_{25}(PET)_{18}^-$ Cluster with Fullerenes. We also tried to form similar adducts of fullerene with $Au_{25}(PET)_{18}^-$,^{10,58,68} which has a core structure similar to that of X^- but protected by a different ligand. $Au_{25}(PET)_{18}$ is referred to as Y in the subsequent discussion. The Y^- cluster was synthesized following the method discussed in the Experimental Section and characterized by UV-vis and ESI MS (Figure S9). Y^- showed the parent cluster ion peak at m/z 7393, as presented in Figure S9B. Upon addition of C_{60} , several new peaks appeared in ESI MS in the m/z range 7500–8300, as presented in Figure 6. The fullerene adducts,

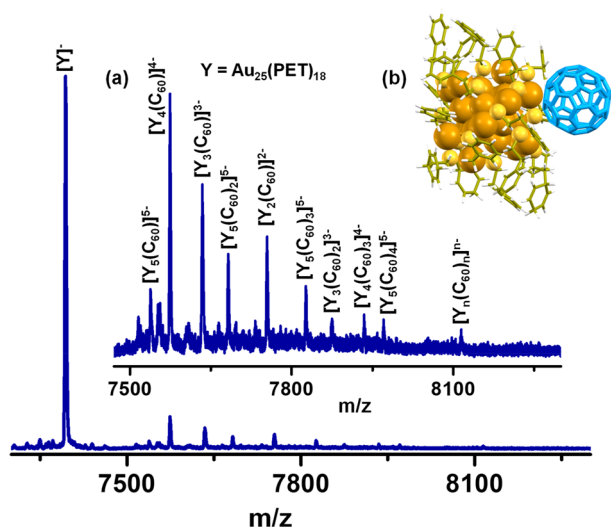


Figure 6. ESI MS showing the formation of adducts of C_{60} with Y^- ($Y = Au_{25}(PET)_{18}$). Expanded view of adducts in the m/z range of 7500–8300 is shown in inset (a), and the DFT-optimized lowest energy structure of $[Y(C_{60})]^-$ is presented in inset (b). Color codes: orange, Au; yellowish-green, C; yellow, S; and white, H.

$[Y_n(C_{60})]^{n-}$ ($n = 1-5$), $[Y_n(C_{60})_{n-1}]^{n-}$ ($n = 2-5$), and $[Y_n(C_{60})_n]^{n-}$ ($n = 1, 2, 3, \dots$, etc.), observed in the case of Y^- , were similar to those observed in the case of X^- . In order to study the nature of complexation and interactions of C_{60} with Y^- , we calculated the structure of $[Y(C_{60})]^-$ using a similar approach used in the case of $[X(C_{60})]^-$. The lowest energy structure of $[Y(C_{60})]^-$ is presented in the inset (b) of Figure 6. $[Y(C_{60})]^-$ showed a B.E. of -12.33 kcal/mol which was marginally higher compared to the B.E. of $[X(C_{60})]^-$ (-10.25 kcal/mol). As the nature of complexation in the case of $[X(C_{60})]^-$ and $[Y(C_{60})]^-$ was similar and independent of the ligands or the metal atoms, ion-induced dipole interaction was expected to be the major driving force behind this complexation. Similar complexation of Y^- with C_{70} was also studied (Figure S10). Our results showed that for an appropriate

geometry of the cluster the complexation was independent of the nature of the metal atoms (Au or Ag), and host–guest complexation was primarily favored by the interaction with the protecting ligands of the cluster and ion-induced dipole interactions.

CONCLUSIONS

In summary, we demonstrated the assembly of atomically precise clusters with fullerenes, C_{60} and C_{70} . Taking $M_{25}(SR)_{18}^-$ ($M = Ag, Au$) clusters as our model systems of study, we showed that fullerene-mediated dimers and trimers and higher aggregates of the clusters were formed, and the nature of complexation was independent of the nature of metal atoms (Ag or Au). The complexation was favored due to ion-induced dipole interactions between the metal clusters and fullerenes and interaction between the protecting ligands of the cluster and the aromatic surface of the fullerenes. Computational studies also supported the formation of such cluster–fullerene complexes and also predicted the possibility of isomerism in some of these adducts. The present study revealed how variation in the structure of the cluster can induce the formation of a variety of cluster–fullerene adducts. The nature of adducts observed in the case of $M_{25}(SR)_{18}^-$ ($M = Ag, Au$) was completely different compared to the previously observed adducts of $[Ag_{29}(BDT)_{12}]^{3-}$ clusters,⁴⁷ where multiple fullerenes were attached to an isolated cluster. Also, our work opens up a methodology to create aggregates of clusters by supramolecular interaction with other molecules. Exploring the interaction of a variety of ligand-protected noble metal clusters with fullerenes can bring in more variation in the nature of supramolecular adducts, which will help to create a large family of such cluster–fullerene hybrid systems. Though we have used clusters protected by hydrophobic ligands in this work, these studies may also be extended to water-soluble metal nanoclusters by using suitable phase transfer agents or by using clusters and fullerenes with appropriate functionalization. Moreover, dimers, trimers, and other aggregates with the fullerenes were formed as a mixture in solution, and selective formation of a particular adduct, containing a desired number of clusters, could not be controlled. Future work will involve separating these aggregates to study their physical and chemical properties. The dimers and trimers may show a change in their mechanical or optical properties. Conductivity may also be observed in the fullerene-mediated aggregates of the clusters. Moreover, the chemical properties of these dimers and trimers may also be altered. These aggregates may behave differently in interparticle reactions,⁶⁰ compared to the monomers of the clusters. Such cluster–fullerene complexes may find applications in diverse fields such as optoelectronics, solar cells, catalysis, etc.

ASSOCIATED CONTENT

Supporting Information

The Supporting Information is available free of charge at <https://pubs.acs.org/doi/10.1021/acs.jpcc.0c03383>.

Optical absorption spectra, additional ESI MS, and computational details (PDF)

AUTHOR INFORMATION

Corresponding Author

Thalappil Pradeep – DST Unit of Nanoscience (DST UNS) and Thematic Unit of Excellence (TUE), Department of

Chemistry, Indian Institute of Technology Madras, Chennai 600 036, India; orcid.org/0000-0003-3174-534X;
Email: pradeep@iitm.ac.in

Authors

Papri Chakraborty – DST Unit of Nanoscience (DST UNS) and Thematic Unit of Excellence (TUE), Department of Chemistry, Indian Institute of Technology Madras, Chennai 600 036, India

Abhijit Nag – DST Unit of Nanoscience (DST UNS) and Thematic Unit of Excellence (TUE), Department of Chemistry, Indian Institute of Technology Madras, Chennai 600 036, India

Biswajit Mondal – DST Unit of Nanoscience (DST UNS) and Thematic Unit of Excellence (TUE), Department of Chemistry, Indian Institute of Technology Madras, Chennai 600 036, India

Esma Khatun – DST Unit of Nanoscience (DST UNS) and Thematic Unit of Excellence (TUE), Department of Chemistry, Indian Institute of Technology Madras, Chennai 600 036, India

Ganesan Paramasivam – DST Unit of Nanoscience (DST UNS) and Thematic Unit of Excellence (TUE), Department of Chemistry, Indian Institute of Technology Madras, Chennai 600 036, India

Complete contact information is available at:
<https://pubs.acs.org/10.1021/acs.jpcc.0c03383>

Notes

The authors declare no competing financial interest.

ACKNOWLEDGMENTS

Authors thank Dr. Anirban Som, Dr. Ganapati Natarajan, Tripti Ahuja, and Korath Shivan Sugi for their help and suggestions in this work. P.C. thanks the Council of Scientific and Industrial Research (CSIR) for a research fellowship. A.N., B.M., and E.K. thank IIT Madras for their Doctoral fellowship. G.P. thanks IIT Madras for an Institute Postdoctoral fellowship. We thank the Department of Science and Technology, Government of India, for providing funding through the grant SR/NM/NS-05/2014(G).

REFERENCES

- (1) Chakraborty, I.; Pradeep, T. Atomically Precise Clusters of Noble Metals: Emerging Link between Atoms and Nanoparticles. *Chem. Rev.* **2017**, *117*, 8208–8271.
- (2) Jin, R.; Zeng, C.; Zhou, M.; Chen, Y. Atomically Precise Colloidal Metal Nanoclusters and Nanoparticles: Fundamentals and Opportunities. *Chem. Rev.* **2016**, *116*, 10346–10413.
- (3) Maity, P.; Xie, S.; Yamauchi, M.; Tsukuda, T. Stabilized Gold Clusters: From Isolation Toward Controlled Synthesis. *Nanoscale* **2012**, *4*, 4027–4037.
- (4) Song, X.-R.; Goswami, N.; Yang, H.-H.; Xie, J. Functionalization of Metal Nanoclusters for Biomedical Applications. *Analyst* **2016**, *141*, 3126–3140.
- (5) Du, X.; Jin, R. Atomically Precise Metal Nanoclusters for Catalysis. *ACS Nano* **2019**, *13*, 7383–7387.
- (6) Ghosh, A.; Mohammed, O. F.; Bakr, O. M. Atomic-Level Doping of Metal Clusters. *Acc. Chem. Res.* **2018**, *51*, 3094–3103.
- (7) Kurashige, W.; Niihori, Y.; Sharma, S.; Negishi, Y. Precise Synthesis, Functionalization and Application of Thiolate-Protected Gold Clusters. *Coord. Chem. Rev.* **2016**, *320–321*, 238–250.
- (8) Du, Y.; Sheng, H.; Astruc, D.; Zhu, M. Atomically Precise Noble Metal Nanoclusters as Efficient Catalysts: A Bridge between Structure and Properties. *Chem. Rev.* **2020**, *120*, 526–622.

(9) Knoppe, S.; Bürgi, T. Chirality in Thiolate-Protected Gold Clusters. *Acc. Chem. Res.* **2014**, *47*, 1318–1326.

(10) Zhu, M.; Aikens, C. M.; Hollander, F. J.; Schatz, G. C.; Jin, R. Correlating the Crystal Structure of a Thiol-Protected Au₂₅ Cluster and Optical Properties. *J. Am. Chem. Soc.* **2008**, *130*, 5883–5885.

(11) Yang, H.; Wang, Y.; Huang, H.; Gell, L.; Lehtovaara, L.; Malola, S.; Häkkinen, H.; Zheng, N. All-Thiol-Stabilized Ag₄₄ and Au₁₂Ag₃₂ Nanoparticles with Single-Crystal Structures. *Nat. Commun.* **2013**, *4*, 2422.

(12) Yan, N.; Xia, N.; Liao, L.; Zhu, M.; Jin, F.; Jin, R.; Wu, Z. Unraveling the Long-Pursued Au₁₄₄ Structure by X-Ray Crystallography. *Sci. Adv.* **2018**, *4*, eaat7259.

(13) Chen, T.; Yao, Q.; Nasaruddin, R. R.; Xie, J. Electrospray Ionization Mass Spectrometry: A Powerful Platform for Noble-Metal Nanocluster Analysis. *Angew. Chem., Int. Ed.* **2019**, *58*, 11967–11977.

(14) Chakraborty, P.; Pradeep, T. The Emerging Interface of Mass Spectrometry with Materials. *NPG Asia Mater.* **2019**, *11*, 48.

(15) Chakraborty, P.; Nag, A.; Chakraborty, A.; Pradeep, T. Approaching Materials with Atomic Precision Using Supramolecular Cluster Assemblies. *Acc. Chem. Res.* **2019**, *52*, 2–11.

(16) Kang, X.; Zhu, M. Intra-Cluster Growth Meets Inter-Cluster Assembly: The Molecular and Supramolecular Chemistry of Atomically Precise Nanoclusters. *Coord. Chem. Rev.* **2019**, *394*, 1–38.

(17) Wu, Z.; Yao, Q.; Zang, S.; Xie, J. Directed Self-Assembly of Ultrasmall Metal Nanoclusters. *ACS Mater. Lett.* **2019**, *1*, 237–248.

(18) Nonappa; Ikkala, O. Hydrogen Bonding Directed Colloidal Self-Assembly of Nanoparticles into 2D Crystals, Capsids, and Supracolloidal Assemblies. *Adv. Funct. Mater.* **2018**, *28*, 1704328.

(19) Rival, J. V.; Nonappa; Shibu, E. S. Light-Triggered Reversible Supracolloidal Self-Assembly of Precision Gold Nanoclusters. *ACS Appl. Mater. Interfaces* **2020**, *12*, 14569–14577.

(20) Shen, J.; Wang, Z.; Sun, D.; Liu, G.; Yuan, S.; Kurmoo, M.; Xin, X. Self-Assembly of Water-Soluble Silver Nanoclusters: Superstructure Formation and Morphological Evolution. *Nanoscale* **2017**, *9*, 19191–19200.

(21) Zeng, C.; Chen, Y.; Kirschbaum, K.; Lambright, K. J.; Jin, R. Emergence of Hierarchical Structural Complexities in Nanoparticles and their Assembly. *Science* **2016**, *354*, 1580–1584.

(22) Gan, Z.; Chen, J.; Wang, J.; Wang, C.; Li, M.-B.; Yao, C.; Zhuang, S.; Xu, A.; Li, L.; Wu, Z. The Fourth Crystallographic Closest Packing Unveiled in the Gold Nanocluster Crystal. *Nat. Commun.* **2017**, *8*, 14739.

(23) Nag, A.; Chakraborty, P.; Bodiuzzaman, M.; Ahuja, T.; Antharjanam, S.; Pradeep, T. Polymorphism of Ag₂₉(BDT)₁₂(TPP)₄³⁻ Cluster: Interactions of Secondary Ligands and Their Effect on Solid State Luminescence. *Nanoscale* **2018**, *10*, 9851–9855.

(24) Baksi, A.; Chakraborty, P.; Bhat, S.; Natarajan, G.; Pradeep, T. [Au₂₅(SR)₁₈]₂²⁻: A Noble Metal Cluster Dimer in the Gas Phase. *Chem. Commun.* **2016**, *52*, 8397–8400.

(25) De Nardi, M.; Antonello, S.; Jiang, D.-e.; Pan, F.; Rissanen, K.; Ruzzi, M.; Venzo, A.; Zoleo, A.; Maran, F. Gold Nanowired: A Linear (Au₂₅)_n Polymer from Au₂₅ Molecular Clusters. *ACS Nano* **2014**, *8*, 8505–8512.

(26) Hossain, S.; Imai, Y.; Motohashi, Y.; Chen, Z.; Suzuki, D.; Suzuki, T.; Kataoka, Y.; Hirata, M.; Ono, T.; Kurashige, W.; et al. Understanding and Designing One-Dimensional Assemblies of Ligand-Protected Metal Nanoclusters. *Mater. Horiz.* **2020**, *7*, 796–803.

(27) Wen, Z.-R.; Guan, Z.-J.; Zhang, Y.; Lin, Y.-M.; Wang, Q.-M. [Au₇Ag₉(Dppf)₃(CF₃CO₂)₇BF₄]_n: A Linear Nanocluster Polymer from Molecular Au₇Ag₈ Clusters Covalently Linked by Silver Atoms. *Chem. Commun.* **2019**, *55*, 12992–12995.

(28) Chakraborty, P.; Baksi, A.; Mudedla, S. K.; Nag, A.; Paramasivam, G.; Subramanian, V.; Pradeep, T. Understanding Proton Capture and Cation-Induced Dimerization of [Ag₂₉(BDT)₁₂]³⁻ Clusters by Ion Mobility Mass Spectrometry. *Phys. Chem. Chem. Phys.* **2018**, *20*, 7593–7603.

- (29) Wei, X.; Kang, X.; Yuan, Q.; Qin, C.; Jin, S.; Wang, S.; Zhu, M. Capture of Cesium Ions with Nanoclusters: Effects on Inter- and Intramolecular Assembly. *Chem. Mater.* **2019**, *31*, 4945–4952.
- (30) Chandra, S.; Nonappa; Beaune, G.; Som, A.; Zhou, S.; Lahtinen, J.; Jiang, H.; Timonen, J. V. I.; Ikkala, O.; Ras, R. H. A. Highly Luminescent Gold Nanocluster Frameworks. *Adv. Opt. Mater.* **2019**, *7*, 1900620.
- (31) Huang, H.-Y.; Cai, K.-B.; Talite, M. J.; Chou, W.-C.; Chen, P.-W.; Yuan, C.-T. Coordination-Induced Emission Enhancement in Gold-Nanoclusters with Solid-State Quantum Yields up to 40% for Eco-Friendly, Low-Reabsorption Nano-Phosphors. *Sci. Rep.* **2019**, *9*, 4053.
- (32) Gayen, C.; Basu, S.; Goswami, U.; Paul, A. Visible Light Excitation-Induced Luminescence from Gold Nanoclusters Following Surface Ligand Complexation with Zn^{2+} for Daylight Sensing and Cellular Imaging. *Langmuir* **2019**, *35*, 9037–9043.
- (33) Shi, J.-F.; Gao, X.-L.; Feng, Y.-H.; Zhou, K.; Ji, J.-Y.; Bi, Y.-F. A $\{Ag_{17}S_8\}$ Cluster-Based Coordination Polymer Linked by Bridging CO_3^{2-} Ligands. *Inorg. Chim. Acta* **2019**, *497*, 119107.
- (34) Nonappa; Lahtinen, T.; Haataja, J. S.; Tero, T.-R.; Häkkinen, H.; Ikkala, O. Template-Free Supracolloidal Self-Assembly of Atomically Precise Gold Nanoclusters: From 2D Colloidal Crystals to Spherical Capsids. *Angew. Chem., Int. Ed.* **2016**, *55*, 16035–16038.
- (35) Lahtinen, T.; Hulkko, E.; Sokołowska, K.; Tero, T.-R.; Saarnio, V.; Lindgren, J.; Pettersson, M.; Häkkinen, H.; Lehtovaara, L. Covalently Linked Multimers of Gold Nanoclusters $Au_{102}(p-MBA)_{44}$ and $Au_{250}(p-MBA)_n$. *Nanoscale* **2016**, *8*, 18665–18674.
- (36) Sokołowska, K.; Luan, Z.; Hulkko, E.; Rameshan, C.; Barrabès, N.; Apkarian, V. A.; Lahtinen, T. Chemically Selective Imaging of Individual Bonds through Scanning Electron Energy-Loss Spectroscopy: Disulfide Bridges Linking Gold Nanoclusters. *J. Phys. Chem. Lett.* **2020**, *11*, 796–799.
- (37) Bodiuzzaman, M.; Nag, A.; Pradeep Narayanan, R.; Chakraborty, A.; Bag, R.; Paramasivam, G.; Natarajan, G.; Sekar, G.; Ghosh, S.; Pradeep, T. A Covalently Linked Dimer of $[Ag_{25}(DMBT)_{18}]^-$. *Chem. Commun.* **2019**, *55*, 5025–5028.
- (38) Sels, A.; Salassa, G.; Cousin, F.; Lee, L.-T.; Bürgi, T. Covalently Bonded Multimers of $Au_{25}(SBut)_{18}$ as a Conjugated System. *Nanoscale* **2018**, *10*, 12754–12762.
- (39) Alhilaly, M. J.; Huang, R.-W.; Naphade, R.; Alamer, B.; Hedhili, M. N.; Emwas, A.-H.; Maity, P.; Yin, J.; Shkurenko, A.; Mohammed, O. F.; et al. Assembly of Atomically Precise Silver Nanoclusters into Nanocluster-Based Frameworks. *J. Am. Chem. Soc.* **2019**, *141*, 9585–9592.
- (40) Wu, X.-H.; Luo, P.; Wei, Z.; Li, Y.-Y.; Huang, R.-W.; Dong, X.-Y.; Li, K.; Zang, S.-Q.; Tang, B. Z. Guest-Triggered Aggregation-Induced Emission in Silver Chalcogenolate Cluster Metal–Organic Frameworks. *Adv. Sci.* **2019**, *6*, 1801304.
- (41) Huang, R.-W.; Wei, Y.-S.; Dong, X.-Y.; Wu, X.-H.; Du, C.-X.; Zang, S.-Q.; Mak, T. C. W. Hypersensitive Dual-Function Luminescence Switching of a Silver-Chalcogenolate Cluster-Based Metal–Organic Framework. *Nat. Chem.* **2017**, *9*, 689–697.
- (42) Sun, L.; Yun, Y.; Sheng, H.; Du, Y.; Ding, Y.; Wu, P.; Li, P.; Zhu, M. Rational Encapsulation of Atomically Precise Nanoclusters into Metal–Organic Frameworks by Electrostatic Attraction for CO_2 Conversion. *J. Mater. Chem. A* **2018**, *6*, 15371–15376.
- (43) Mathew, A.; Natarajan, G.; Lehtovaara, L.; Häkkinen, H.; Kumar, R. M.; Subramanian, V.; Jaleel, A.; Pradeep, T. Supramolecular Functionalization and Concomitant Enhancement in Properties of Au_{25} Clusters. *ACS Nano* **2014**, *8*, 139–152.
- (44) Nag, A.; Chakraborty, P.; Paramasivam, G.; Bodiuzzaman, M.; Natarajan, G.; Pradeep, T. Isomerism in Supramolecular Adducts of Atomically Precise Nanoparticles. *J. Am. Chem. Soc.* **2018**, *140*, 13590–13593.
- (45) Bhunia, S.; Kumar, S.; Purkayastha, P. Gold Nanocluster-Grafted Cyclodextrin Suprastructures: Formation of Nanospheres to Nanocubes with Intriguing Photophysics. *ACS Omega* **2018**, *3*, 1492–1497.
- (46) Yan, C.; Liu, C.; Abroshan, H.; Li, Z.; Qiu, R.; Li, G. Surface Modification of Adamantane-Terminated Gold Nanoclusters Using Cyclodextrins. *Phys. Chem. Chem. Phys.* **2016**, *18*, 23358–23364.
- (47) Chakraborty, P.; Nag, A.; Paramasivam, G.; Natarajan, G.; Pradeep, T. Fullerene-Functionalized Monolayer-Protected Silver Clusters: $[Ag_{29}(BDT)_{12}(C_{60})_n]^{3-}$ ($n = 1–9$). *ACS Nano* **2018**, *12*, 2415–2425.
- (48) Chakraborty, P.; Nag, A.; Sugi, K. S.; Ahuja, T.; Varghese, B.; Pradeep, T. Crystallization of a Supramolecular Coassembly of an Atomically Precise Nanoparticle with a Crown Ether. *ACS Mater. Lett.* **2019**, *1*, 534–540.
- (49) Muhammed, M. A. H.; Cruz, L. K.; Emwas, A.-H.; El-Zohry, A. M.; Moosa, B.; Mohammed, O. F.; Khashab, N. M. Pillar[5]Arene-Stabilized Silver Nanoclusters: Extraordinary Stability and Luminescence Enhancement Induced by Host–Guest Interactions. *Angew. Chem., Int. Ed.* **2019**, *58*, 15665–15670.
- (50) Wang, J.; Lin, X.; Shu, T.; Su, L.; Liang, F.; Zhang, X. Self-Assembly of Metal Nanoclusters for Aggregation-Induced Emission. *Int. J. Mol. Sci.* **2019**, *20*, 1891.
- (51) Haddon, R. C. Electronic Structure, Conductivity and Superconductivity of Alkali Metal Doped (C_{60}). *Acc. Chem. Res.* **1992**, *25*, 127–133.
- (52) Wang, Y.; Cheng, L. T. Nonlinear Optical Properties of Fullerenes and Charge-Transfer Complexes of Fullerenes. *J. Phys. Chem.* **1992**, *96*, 1530–1532.
- (53) Holczer, K.; Klein, O.; Huang, S.-m.; Kaner, R. B.; Fu, K.-j.; Whetten, R. L.; Diederich, F. Alkali-Fulleride Superconductors: Synthesis, Composition, and Diamagnetic Shielding. *Science* **1991**, *252*, 1154.
- (54) Pinkard, A.; Champsaur, A. M.; Roy, X. Molecular Clusters: Nanoscale Building Blocks for Solid-State Materials. *Acc. Chem. Res.* **2018**, *51*, 919–929.
- (55) Roy, X.; Lee, C.-H.; Crowther, A. C.; Schenck, C. L.; Besara, T.; Lalancette, R. A.; Siegrist, T.; Stephens, P. W.; Brus, L. E.; Kim, P.; et al. Nanoscale Atoms in Solid-State Chemistry. *Science* **2013**, *341*, 157.
- (56) Schulz-Dobrick, M.; Jansen, M. Intercluster Compounds Consisting of Gold Clusters and Fullerenes: $[Au_7(PPh_3)_7]C_{60}$ -THF and $[Au_8(PPh_3)_8](C_{60})_2$. *Angew. Chem., Int. Ed.* **2008**, *47*, 2256–2259.
- (57) Joshi, C. P.; Bootharaju, M. S.; Alhilaly, M. J.; Bakr, O. M. $[Ag_{25}(SR)_{18}]^-$: The “Golden” Silver Nanoparticle. *J. Am. Chem. Soc.* **2015**, *137*, 11578–11581.
- (58) Heaven, M. W.; Dass, A.; White, P. S.; Holt, K. M.; Murray, R. W. Crystal Structure of the Gold Nanoparticle $[N(C_8H_{17})_4]-[Au_{25}(SCH_2CH_2Ph)_{18}]$. *J. Am. Chem. Soc.* **2008**, *130*, 3754–3755.
- (59) Zhu, M.; Lanni, E.; Garg, N.; Bier, M. E.; Jin, R. Kinetically Controlled, High-Yield Synthesis of Au_{25} Clusters. *J. Am. Chem. Soc.* **2008**, *130*, 1138–1139.
- (60) Krishnadas, K. R.; Ghosh, A.; Baksi, A.; Chakraborty, I.; Natarajan, G.; Pradeep, T. Intercluster Reactions between $Au_{25}(SR)_{18}$ and $Ag_{44}(SR)_{30}$. *J. Am. Chem. Soc.* **2016**, *138*, 140–148.
- (61) Morris, G. M.; Huey, R.; Lindstrom, W.; Sanner, M. F.; Belew, R. K.; Goodsell, D. S.; Olson, A. J. Autodock4 and Autodocktools4: Automated Docking with Selective Receptor Flexibility. *J. Comput. Chem.* **2009**, *30*, 2785–2791.
- (62) Mortensen, J. J.; Hansen, L. B.; Jacobsen, K. W. Real-Space Grid Implementation of the Projector Augmented Wave Method. *Phys. Rev. B: Condens. Matter Mater. Phys.* **2005**, *71*, No. 035109.
- (63) Enkovaara, J.; Rostgaard, C.; Mortensen, J. J.; Chen, J.; Dulak, M.; Ferrighi, L.; Gavnholt, J.; Glinsvad, C.; Haikola, V.; Hansen, H. A.; et al. Electronic Structure Calculations with Gpaw: A Real-Space Implementation of the Projector Augmented-Wave Method. *J. Phys.: Condens. Matter* **2010**, *22*, 253202.
- (64) Perdew, J. P.; Burke, K.; Ernzerhof, M. Generalized Gradient Approximation Made Simple. *Phys. Rev. Lett.* **1996**, *77*, 3865–3868.
- (65) Chakraborty, P.; Baksi, A.; Khatun, E.; Nag, A.; Ghosh, A.; Pradeep, T. Dissociation of Gas Phase Ions of Atomically Precise

Silver Clusters Reflects Their Solution Phase Stability. *J. Phys. Chem. C* **2017**, *121*, 10971–10981.

(66) Dugourd, P.; Antoine, R.; Rayane, D.; Compagnon, I.; Broyer, M. Enhanced Electric Polarizability in Metal C_{60} Compounds: Formation of a Sodium Droplet on C_{60} . *J. Chem. Phys.* **2001**, *114*, 1970–1973.

(67) Musnier, B.; Wegner, K. D.; Comby-Zerbino, C.; Trouillet, V.; Jourdan, M.; Häusler, I.; Antoine, R.; Coll, J.-L.; Resch-Genger, U.; Le Guével, X. High Photoluminescence of Shortwave Infrared-Emitting Anisotropic Surface Charged Gold Nanoclusters. *Nanoscale* **2019**, *11*, 12092–12096.

(68) Kang, X.; Chong, H.; Zhu, M. $Au_{25}(SR)_{18}$: The Captain of the Great Nanocluster Ship. *Nanoscale* **2018**, *10*, 10758–10834.